

Measurement of plasma characteristics of the optically generated copper plasma by laser spectroscopy technique

RABIA QINDEEL^a, WALID TAWFIK^{a,b,*}

^aPhysics and Astronomy Department, King Saud University, Riyadh 11451, Saudi Arabia

^bNational Institute of Laser Enhanced Sciences NILES, Department of Environmental Applications, Cairo University, Cairo, Egypt

Laser-induced breakdown spectroscopy (LIBS) or laser induced plasma spectroscopy (LIPS) technique has been applied to investigate plasma characterization of pure copper in air. The fundamental wavelength of Q-switched Nd:YAG laser beam was focused on the copper target with intensity of about 6.6×10^8 W/cm² to generate the plasma. The laser intensity was optimized to avoid air breakdown on the target surface. The generated Cu plasma plume was monitored with CCD camera and the emission is analyzed with an Ophir WaveStar spectrometer. The plasma temperature is calculated as 10100 K while plasma density is 5.4×10^{17} cm⁻³. The CCD observed image of the constructed plasma plume showed that it is oblate shape rather than expected spherical nature. The observed results revealed the spatial distribution of the generated plasma plume expansion towards the laser beam that depends on the plasma properties. The observed ablation profile with the number of laser pulses is also studied.

(Received March 14, 2014; accepted July 10, 2014)

Keywords: Laser induced Breakdown, Copper, Plasma parameters

1. Introduction

In the recent years, Laser Induced Breakdown Spectroscopy (LIBS) represents one of the most important analytical techniques for a variety of samples. Thus LIBS can be applied for industrial applications (materials analysis), environmental applications (soil and water), medical applications (tissue, teeth, and bones), and art conservation (ancient metals, pigments). LIBS technique is based on the spectral analysis of the radiation emitted by plasma generated by focusing an intense laser pulse on the sample (gas, liquid or solid). The high intensity of laser beam ($\sim 10^8$ W/cm²) ablates and ionizes a small amount of the sample material and then consequently a micro-plasma is formed. The emission spectra of the generated plasma gives details about the sample composition and the plasma characterization. Subsequently each laser pulse, both of cooling process of the plasma produces electron recombination and atom de-excitation take place. LIBS spectra can be observed as soon as the plasma continuum emission is almost surpassed. The advantages of this spectroscopic technique have been reviewed in several papers [1-5]. The laser beam can be guided using optical fibers to collect the generated emitted plasma emission. The later facilitate remote LIBS system that permits investigation of hazard targets as well as is difficult access samples [6]. Thus by using of telescopes the collection of the plasma plume emissions can be achieved for long distances between target, sample and diagnostic system via standoff LIBS system [7].

The study of laser-induced plasma has been investigated by examining emission characteristics of the generated plasma to apply this technique for the analysis of atomic species [8]. Several scientists have been studied the performances of the laser induced plasma by varying the gas pressure, buffer gases, the laser intensity, and many interesting observations were published [9-10]. It is concluded that the laser-induced plasma is regarded to have two main zones, inner sphere-zone and outer sphere-zone. The inner sphere-zone has a high density of ionic and atomic species that intensity of emission is high, while many ionic emission-bands exist as a noise background factor in emission spectra. The outer sphere-zone has a low population-density of ionic species and the emission intensity is relatively weaker. Research group Kagawa et al. have considered the effect of atmosphere and laser energy on the plasma emission characteristics, and the optimum condition for the maximum intensity of the elemental emissions [11]. It is concluded that the blast wave explosion model could explain the ablation process for the solid materials.

In the current study, we have investigated the plasma produced by Nd:YAG laser 1064 nm nanosecond pulse focused on pure copper target in air. Pure copper is selected as a solid material and to avoid matrix effects of the impurities. We have considered the plasma electron temperature of the generated plasma using Boltzmann plot method and the electron density via the Stark broadening. Furthermore, the stoichiometry of the ablated plume at different number of pulses is studied.

2. Materials and methods

2.1 Experimental setup

The plasma were generated by Nd:YAG laser. The laser beam from a Q-switched Nd:YAG laser with pulse duration of 8 ns, 1064 nm wavelength, pulse energy 166 mJ and power density of $6.6 \times 10^8 \text{ W cm}^{-2}$ was used to irradiate the Cu target. The spot size of the laser on the

target is about 1 mm. Cu plate is used as a target material with $1 \times 1 \text{ cm}$ dimension. A cylindrical lens was used to image the laser induced plasma 1:1 onto the entrance slit of a spectrometer with the slit width set to $10 \mu\text{m}$. The spectra is recorded with spectrum analyser. The acquired emission data by Ophir WaveStar spectrometer (CCD laser spectrum analyzer) have been stored in a PC using WaveStar 1.05 software for subsequent analysis. The experimental setup is shown in Fig. 1.

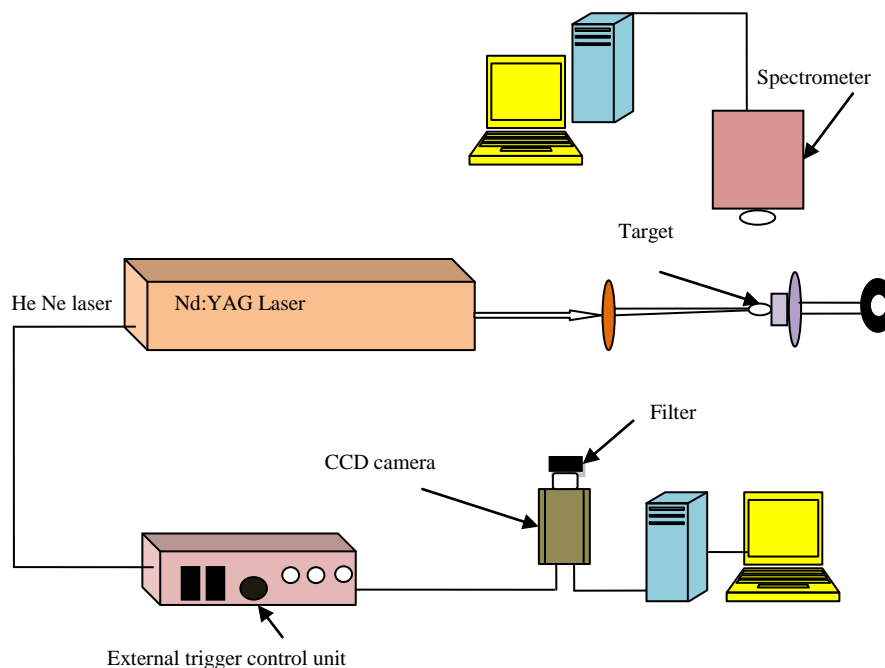


Fig. 1. Schematic of the experimental setup.

2.2 Spectrum analysis

Optical emission or radiations of the plasma of different target material is analyzed through Ophir WaveStar spectrometer. The Ophir WaveStar (Fig. 2) introduces a new level of accuracy and ease in spectral measurements. The WaveStar program automatically tags the peaks with the wavelength so the result is readily available. The WaveStar has up to 4 times as high resolution as similar competing instruments due to its innovative optical design. Its innovative peak interpolation algorithms allows to find the peak wavelengths of lines at up to 10 times the accuracy of competing instruments. The built in intensity calibration insures that the relative intensity vs. wavelength gives an accurate relative curve.



Fig. 2. Ophir WaveStar spectrometer.

2.3 The sample

The used solid sample was pure copper 99.99 % disks (Singapore International chemical Co., Ltd. Singapore).

3. Results and discussion

3.1 LIBS spectrum

The laser energy was optimized in this experiment to avoid the ambient air breakdown influence on the copper LIBS spectrum. This is achieved by optimizing the laser energy using 1064 nm laser of 8 ns pulse duration focused with lens of 10 cm focal length. We found that using 166 mJ laser energy produce a beam waist $w_0 \sim 1$ mm FWHM at the surface of the sample. This in turn gives laser intensity of 6.6×10^8 W/cm² which is much lower than the breakdown threshold of 1064 nm in air ($\sim 1 \times 10^{11}$ W/cm²) [12-14]. In addition, we did not detect any significant emission atomic lines of oxygen or nitrogen in our LIBS

spectrum of our samples. This indicates that environmental influences have been fully avoided due to optimized experimental conditions. The observed LIBS spectrum of copper sample in the range 420- 580 nm is shown in Fig. 2. In the present study, different emission lines from atomic isolated cu lines and does not interfere with any other lines as shown in Fig. 2. The lines of observed elements are marked in Fig. 2 and listed with its spectroscopic data in table 1. The assignment of these lines is done using the NIST database [15]. A partial energy level diagram for excited copper Cu(I) lines showing the important transitions responsible for the emission of the laser produced plasma in the range 420 – 580 nm is shown in Fig. 4.

Table 1. Spectroscopy parameters of neutral Cu transitions lines in the observed LIBS spectrum.

Wavelength λ (nm)	Transition lines	Statistical Weight	Transition Probability A_{ij} ($\times 10^8$ s ⁻¹)	Energy of the Upper Level
λ (nm)		g_i	A_{ij} (s ⁻¹)	E_k (cm ⁻¹)
427.45	$3d^9 4s 5s^2 D_{3/2} \rightarrow 3d^9 4s 5s^2 F_{5/2}$	8	0.34	62403.32
465.1	$3d^9 4s 5s^2 D_{3/2} \rightarrow 3d^9 4s 5s^2 F_{5/2}$	8	0.38	62403.32
510.46	$3d^{10} 4p^2 P_{3/2} \rightarrow 3d^9 4s^2 D_{5/2}$	4	0.020	30783.686
515.20	$3d^{10} 4d^2 D_{3/2} \rightarrow 3d^{10} 4p^2 P_{1/2}$	4	0.60	49935.200
521.71	$3d^{10} 4d^2 D_{5/2} \rightarrow 3d^{10} 4p^2 P_{3/2}$	6	0.75	49942.057
578.21	$3d^{10} 4p^2 P_{3/2} \rightarrow 3d^9 4s^2 D_{3/2}$	2	0.016	30535.302

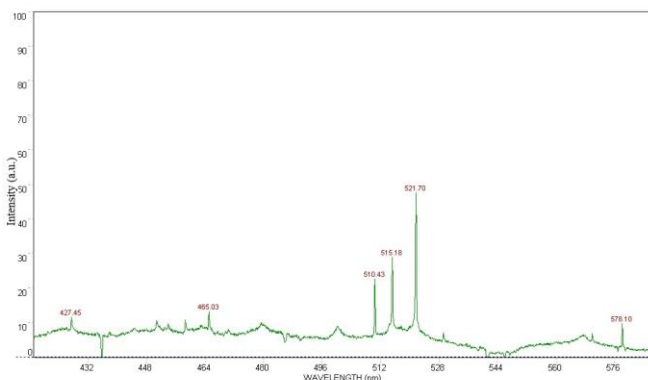


Fig. 3. LIBS spectrum of pure Copper in air.

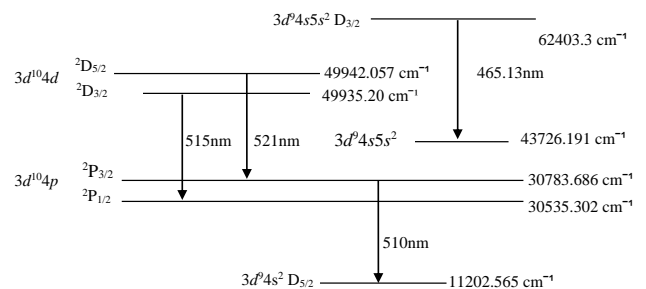


Fig. 4. Partial energy level diagram of Cu showing the most probable observed transition.

3.2 Plasma parameters

In order to provide accurate consideration of plasma parameters, the local thermodynamic equilibrium (LTE) plasma assumption should be confirmed. Thus parameters

such as plasma temperatures and electron density have to be measured and compared with the LTE condition.

Under the LTE assumption, the electron dominates the reaction rate, so the measured emission line intensity of a single species is resulting from the Boltzmann equation as:

$$I_{\lambda} = F.C_s \frac{A_{ki} g_k}{U_s(T)} \exp\left(-\frac{E_k}{KT}\right) \quad (1)$$

Where A_{ki} and g_k are respectively the transition probability and the statistical weight for the upper level. T is the temperature, E_k is the excited level energy, and K is the Boltzmann constant. C_s is the species concentration, $U(T)$ is the partition function, and F is an experimental factor. By taking the logarithm of eq. (1), we got a linear relationship:

$$\ln \frac{I_k}{A_{ki} g_k} = -\frac{1}{KT} . E_k + \ln \frac{C_s F}{U_s(T)} \quad (2)$$

A plot of the relation on the left side vs. E_k has a slope of $-1/KT$. Therefore, the T plasma temperature can be observed without expressive F , or the partition function $U(T)$. A typical Boltzmann plot of cu lines is shown in Fig. 5. The curve slope yield a temperature of 10100 K.

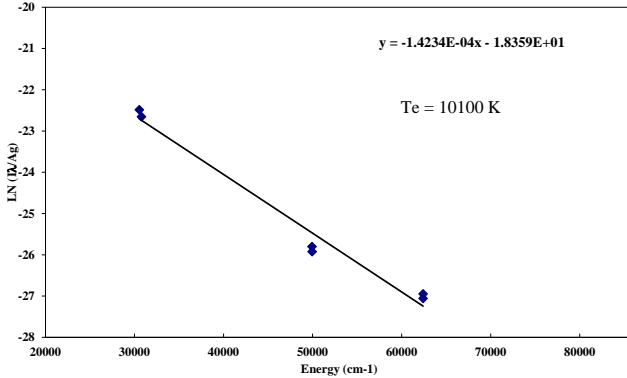


Fig. 5. Boltzmann plot for the calculation of the excitation temperature of Cu I.

Electron density could be measured by determine the line profile [16]. Under our condition the main contribution to line width is related to the stark broadening; the line profile for stark broadened is well represented by a Lorentz function.

Meanwhile the instrumental line-broadening show Lorentz shape, the stark line width can be determined from the measured line width by deducting the instrumental line-broadening:

$$\Delta\lambda = \Delta\lambda_{obs.} - \Delta\lambda_{inst.} \quad (3)$$

It was found for our setup that $\Delta\lambda_{inst}$ was 0.05nm (determined by determining the FWHM of the Hg lines emitted by a spectral lamp).

It is well known that the width of stark broadening spectral line be determined by the electron density N_e [17]. Both the quadratic and the linear stark effect are considered in spectroscopy. Only the hydrogen atom and H-like ion reveal the linear stark effect. For the linear-stark effect the electron density should be realized from H line width from the formula [17]

$$N_e = C(N_e, T) . \Delta\lambda_{FWHM}^{3/2} \quad (4)$$

the constant $C(N_e, T)$ for H line is tabulated in the literature, the $\Delta\lambda$ is in Angstrom [18].

For non-H-like line, the electron density could be determined from the FWHM of the line from the formula [16]:

$$N_e \approx \left(\frac{\Delta\lambda_{FWHM}}{2.w} \right) . 10^{16}. \quad (5)$$

Which is generally used for calculations of plasma generated from solid targets. w is the electron impact parameter and it can be find in well documented tables [18].

For the cu 465.1 nm line, it was found that $w = 4.1 \times 10^{-3}$ nm [19] and $\Delta\lambda_{FWHM}$ measured from Fig. 3 using lorentzian curve fitting and found to be $\Delta\lambda_{FWHM} = 0.5$ nm, so from eq (3) the net width is $\Delta\lambda = 0.45$ nm and by substituting in eq. (5) then copper plasma electron density $N_e = 5.48 \times 10^{17}$ cm⁻³.

The lower limit for electron density for which the plasma will be in LTE is:

$$N_e \geq 1.6 . 10^{12} . \Delta E . T^{1/2} \quad (6)$$

ΔE is the largest energy transition for which the condition holds.

In our case $\Delta E = 2.66$ eV for cu 465.1 nm for transition $3d^9 4s 5s^2 D_{3/2} \rightarrow 3d^9 4s 5s^2 F_{5/2}$ (Table 1) and the electron density lower limit value given by Eq. (6) is 4.27×10^{14} cm⁻³. The measured density (5.48×10^{17} cm⁻³) is found to be greater than this value, which is consistent with the assumption of LTE prevailing in the plasma. The later confirm the LTE condition for the observed plasma copper.

3.3 Plume image and ablation profile

Plasma plume emission starts on the copper target surface soon after the laser photons reach the surface. Images of the time integrated evolution of the expanding copper plasma was taken at as a side view. Typical CCD image of the expanding plume at after the onset of plasma starts is given in Fig. 6. This image was recorded at laser irradiance of 6×10^8 W/cm². The CCD observed image of

the constructed plasma plume showed that it is oblate shape rather than expected spherical nature. The observed results revealed the spatial distribution of the generated

plasma plume expansion towards the laser beam that depends on the plasma properties.

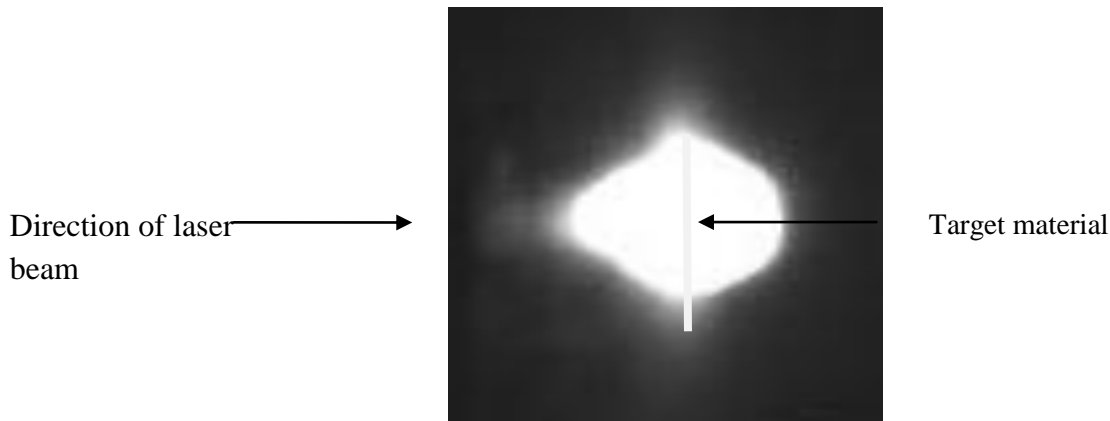
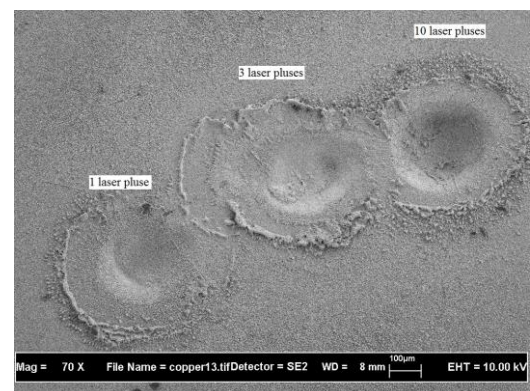


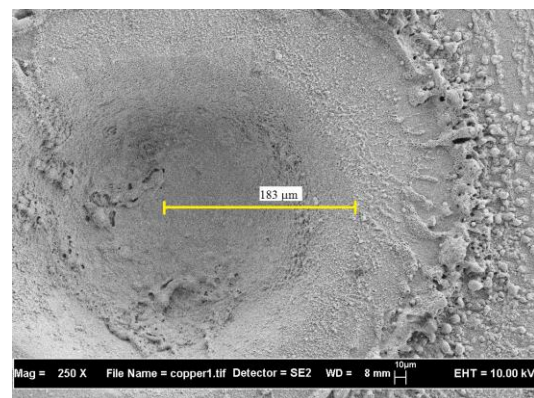
Fig. 6. Plasma plume image.

The generated plasma made craters on the copper sample surface. The formed crater depends on laser parameters such as wavelength, fluence, pulse duration, and pulse repetition rate. A standard scanning electron microscope (SEM) was used to monitor the morphology and depth profile of each crater [20]. Fig. 7 shows typical two-dimensional images of craters formed on the surface of pure copper sample. Fig. 7 (a) reveals the one, three, and ten laser pulses top view, while Fig. 7 (b) represents a zoomed image of the ten pulses crater estimated measurement of its depth of 183 μm . Visually, it can be estimated that the crater depth profile increased with the number of laser pulses. Furthermore, laser-breakdown parameters such as electron density, temperature and optical emission intensity could play important role in the depth and shape of the generated crater. This is because when laser light falls on copper surface, the free electrons will be excited. The electronic excitation energy is then converted into kinetic energy of lattice vibrations. The collision frequency of electron-ion will increase with an increase in electron temperature.

Ablation may happens if the energy deposited in delocalized phonons surpasses the critical temperature at which phase transformation arises. Consequently, hot plasma and high-density are desirable for efficient ablation and more surface modification. This will be verified in the future experiments by using a varied laser intensity source for different wavelengths. This study will be accomplished with using gated ICCD camera for time resolved measurements, which will reveal more about plasma plume expansion with time with varied laser parameters.



a



b

Fig. 7. SEM images of the craters formed on copper surface using different numbers of Nd:YAG laser pulses. (a) 1 pulse, 3 pulses, and 10 pulses top view. (b) zoomed image of the crater due to 10 laser pulses.

5. Conclusion

In this study, LIBS technique was used to study the plasma characteristics of the generated plasma of pure copper sample. The laser intensity was reduced to avoid the ambient air breakdown which may influence the copper plasma emission lines. The observed LIBS spectrum revealed well resolved copper spectral lines in the spectral range from 420-580 nm. The plasma temperature reaches 10100 k while density reaches $5.4 \times 10^{17} \text{ cm}^{-3}$. The plasma plume is found to have oblate shape and expanded towards the laser beam. The observed ablation depth increases with the number of laser pulses. The obtained result is important for some industrial applications, such as controlling thin-film lithography and online measurements of pulsed laser deposition techniques.

Acknowledgement

This project is supported by King Saud University, Deanship of Scientific Research, College of Science Research Center.

References

- [1] J. P. Singh, S. N. Thakur, Elsevier Science, (2007).
- [2] L. J. Radziemski, T. R. Loree. *Plasma Chemistry and Plasma Processing*. **1**(3), 281 (1981).
- [3] D. Anglos, S. Couris, C. Fotakis. *Applied Spectroscopy*, **51**(7), 1025 (1997).
- [4] J. M. Vadillo, J. J. Laserna, *Spectrochim. Acta B* **59**, 147–161. Majidi V, Joseph M R. 1992, *Crit. Rev. Anal. Chem.* **23**, 143 (2004).
- [5] J. P. Singh, S. N. Thakur, Elsevier Science, (2007) ISBN: 978-0-444-51734-0.
- [6] C. Lopez-Moreno, S. Palanco, J. J. Laserna, F. DeLucia Jr, A. W. Miziolek, J. Rose, R. A. Walters, A. I. Whitehouse, *J. Anal. At. Spectrom.* **21**(1), 55-60 Portnov A, Rosenwaks S, Bar I. 2003, *Appl. Opt.* **42**, 2835 (2005).
- [7] G. Bazalgette Courra ges-Lacoste, B. Ahlers, F. R. Parez, *Spectrochimica Acta Part A: Molecular and Biomolecular Spectroscopy* **68**(4), 1023 (2007).
- [8] K. J. Grant, G. L. Paul, J. A. O'Neill, *Applied Spectroscopy*, **45**, 701 (1991).
- [9] Nazar Farid, Shazia Bashir, Khaliq Mahmood, *Phys. Scr.* **85**, 015702 (2012).
- [10] Matthieu Baudelet, Christina C. C. Willis, Lawrence Shah, Martin Richardson *Optics Express*, **18**(8), 7905 (2010).
- [11] K. Kagawa, K. Kawai, M. Tani, T. Kobayashi, *Applied Spectroscopy*, **48**, 198 (1994).
- [12] P. L. Kelley, B. Lax, P. E. Tannenwald, *Research USOoN. Physics of Quantum Electronics: Conference Proceedings: McGraw-Hill; 1966.*
- [13] M. Thiyagarajan, S. Thompson, *J Appl Phys.* **111**(7), (2012).
- [14] D. E. Lencioni, *Appl Phys Lett.*; **25**(1), 15 (1974).
- [15] A. Kramida, Yu. Ralchenko, Reader, J., and NIST ASD Team (2013). NIST Atomic Spectra Database (ver. 5.1). <http://physics.nist.gov/asd>
- [16] W. T. Mohamed, *Optica Applicata*. **37**(1-2), 5 (2007).
- [17] T. Y. Mohamed Walid, *Opt Laser Technol.* **40**(1), 30 (2008).
- [18] H. R. Griem, *Plasma spectroscopy: McGraw-Hill;* (1964).
- [19] N. Konjević, W. L. Wiese, *J. Phys. Chem. Ref. Data* **19**, 1337 (1990).
- [20] <http://www.jeolusa.com/> (JEOL model JSM-5900LV).

*Corresponding author: wmohamed@ksu.edu.sa